

# Correlation between Peak Spatial-Average SAR and Temperature Increase Due to Antennas Attached to Human Trunk

Akimasa Hirata, *Member, IEEE*, Osamu Fujiwara, *Member, IEEE*, and Toshiyuki Shiozawa, *Fellow, IEEE*

**Abstract**—This paper discusses the correlation between peak spatial-average SAR and maximum temperature increase for antennas attached to the human trunk. Frequency bands considered are 150 MHz, 400 MHz, and 900 MHz, which are assigned for occupational communications. This problem is thoroughly investigated with the aid of Green's function. In particular, the effect of variation of thermal constants on the temperature increase is revealed by using one-dimensional model. Computational results suggests that one of the most dominant factors which affect the correlation between peak SAR and maximum temperature increase is blood flow in tissues. This is confirmed by considering a 3-D realistic human body model. Uncertainties caused by the calculation of peak SAR and the difference in the body model shape are also quantified.

**Index Terms**—blood flow, Green's function, specific absorption rate (SAR), temperature increase

## I. INTRODUCTION

IN recent years, much attention has been paid to health implication of electromagnetic (EM) waves. Mobile telephones are singled out since they have been spread rapidly and are used in close proximity to the user's head. According to safety guidelines (e.g., [1]), peak spatial-average SAR is used as a measure for human protection from RF near field exposures.

One of the dominant effects caused by microwave absorption is a temperature increase. The temperature increase at the safety limit of the guidelines has not yet been investigated sufficiently. The threshold temperature of the pricking pain in the skin is 45 °C, corresponding to the temperature increase of 10-15 °C [2]. Long-time exposure at this level results in burning. It is also reported that a temperature increase in the hypothalamus of 0.2 °C – 0.3 °C leads to altered thermoregulatory behavior [3]. Therefore, the temperature increase in the anatomically-based human head model due to handset antennas has been calculated in several works [4], [5], [6], [7], [8], [9], [10]. In particular, we have revealed that maximum temperature increases in the head and brain are approximately proportional to peak SARs in the corresponding regions [10].

Little attention has been paid to the case where a mobile terminal is attached to a trunk. This situation often happens in

occupational wireless communications [11], [12], [13], [14]. There are main three differences between occupational and commercial use. Firstly, occupational mobile terminals are mainly attached to the trunk. Then, tissue constitution largely depends on the location where a wireless terminal is installed. Common locations are neck/back [11], [12], [14] and waist [13], while that depends on individual users. A temperature increase around the body surface becomes essential, unlike the case of public cellular telephone, since no important organ, such as eye, brain, and so forth, exists in the trunk. Secondly, main frequency bands are 150, 400, 900 MHz, which are different with regulations in each country. The point to be stressed is that these frequency bands are lower than (at least comparable to) those of public commercial applications, such as GSM, PDC, IMT-200 (900MHz-2.2GHz), and so forth. This results in different SAR distribution, since the penetration depth of EM waves becomes small with the increase of the frequency. Furthermore, maximum permissible exposure in occupational environment is five times larger than that in public environment, leading to larger temperature increase.

In this paper, first, we discuss fundamental characteristics of temperature increases in human tissues for heat source in terms of a Green's function [15], [16]. Particularly, a one-dimensional model is used to give some insight for the Green's function. Additionally, we investigate the SAR and temperature increase in the human body due to different antennas, which are placed in proximity to different parts of the trunk: neck, waist, and back. Our attention is paid to uncertainties caused by the blood flow of tissues and the body model shape.

## II. METHODS AND MODEL

### A. Model

The human body model used in this paper is obtained from the Internet Site of Brooks Air Force Base [17]. It consists of  $96 \times 110 \times 125$  cubic cells, whose side cell length is 3.0 mm. This model is comprised of 38 tissues, that is, skin, bone, muscle, fat, nerve, blood, and so forth.

### B. FDTD method and Wave Source

The FDTD method [18] is used for investigating interaction between the human body model and EM waves. In order to incorporate the inhomogeneous head model into the FDTD scheme, the dielectric properties of the tissues are required.

Manuscript received January 20, 2002; revised November 18, 2002. This work was partially supported by Grant-in-Aid for Young Scientist (B), Japan Society for the Promotion of Science.

A. Hirata and O. Fujiwara are with the Department of Electrical and Computer Engineering, Nagoya Institute of Technology, Nagoya 466-8555, Japan. T. Shiozawa is with Department of Electronics and Information Engineering, Chubu University, Aichi 487-8501, Japan.

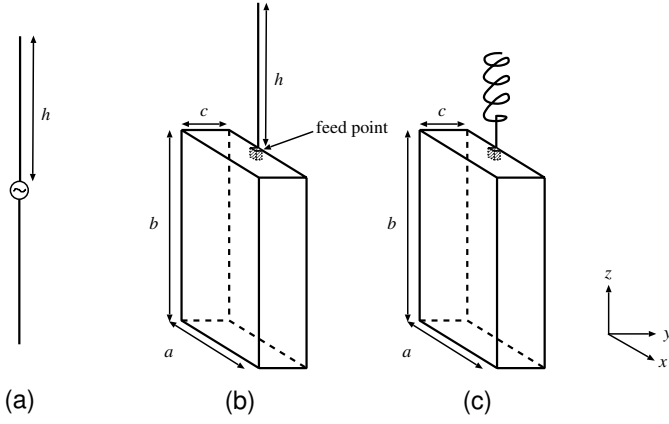


Fig. 1. (a) Dipole antenna and monopole antenna on the metallic box:  $a = 60$  mm,  $b = 180$  mm, and  $c = 30$  mm.

They are determined with the aid of the 4-Cole-Cole extrapolation [19]<sup>1</sup>. It should be noted that 2/3 muscle is considered as a homogeneous medium. The electrical constants of this tissue is defined as those of muscle multiplied by a factor of 2/3. This material is often used in the computational dosimetry, since the ratio of high-water content tissue to low-water content tissue in humans is approximately 2:1. This would not be exception in the trunk.

As wave sources, a dipole antenna, monopole and helical antennas on a metallic box are considered as shown in Fig. 1. For feeding the dipole and monopole antennas, infinitesimal small gap method is used [20], while a stack model is used for the helical antenna [21]. The frequency bands are 400 MHz and 900 MHz for the dipole and monopole antennas. The diameter of the dipole antenna is fixed to 1.0 mm, and the length fixed to 360 mm for 400 MHz and 150 mm for 900 MHz, respectively. The diameter of the monopole antenna is the same as that of the dipole antenna. The dimension of the metallic box is 60 ( $x$ ) X 30 ( $y$ ) X 180 ( $z$ ) mm. The length of  $h$  is also the same as that of the dipole antenna. For the helical antenna, the frequency bands considered are 150 MHz and 400 MHz. The diameter and pitch of the helix are 10 mm and 2 mm for both frequencies, while its length is 60 mm at 150 MHz and 25 mm at 400 MHz. The output power is 1.0 W. Three positions of the antennas relative to the body are considered to be behind the back, waist, and neck of the body (See Fig. 2).

### C. Temperature Calculation

The temperature in the human body is calculated by solving the bioheat equation. The SAR calculated by the FDTD method is used as the heat source [4], [6]. The bioheat equation [22], [23], which takes into account the heat exchange mechanisms such as heat conduction, blood flow, and EM heating, is represented by the following equation:

$$C(\mathbf{r})\rho(\mathbf{r})\frac{dT(\mathbf{r},t)}{dt} = \nabla \cdot (K(\mathbf{r})\nabla T(\mathbf{r},t)) + \rho(\mathbf{r})(\text{SAR}(\mathbf{r})) + Q(\mathbf{r}) - B(\mathbf{r})(T(\mathbf{r},t) - T_B) \quad (1)$$

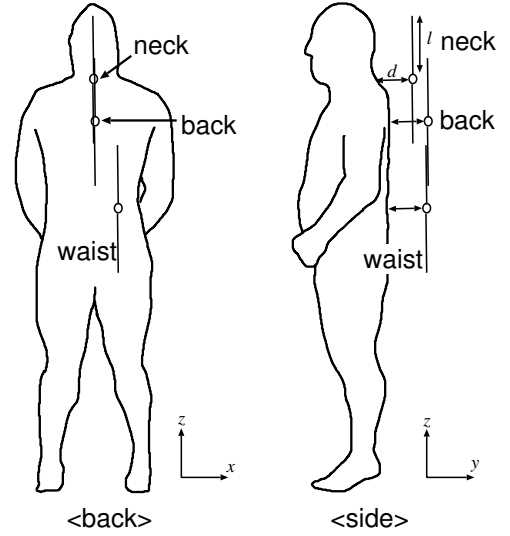


Fig. 2. Positions of antennas relative to the human body model.

where  $T$  is the temperature of the tissue,  $K$  the thermal conductivity of the tissue,  $C$  the specific heat of the tissue,  $Q$  metabolic heat generation, and  $B$  the term associated with blood flow. These parameters are listed in Table I. The temperature increase due to the antennas is assumed to be so small that it cannot activate the thermoregulatory mechanism: the increase of local blood flow, the activation of sweating mechanism, and so forth. Thus, this effect is neglected in our discussion. The effectiveness of this assumption will be commented in Sec. 3.2. The boundary condition for Eq. (1) is given by

$$H \cdot (T_s(\mathbf{r}) - T_e) = -K(\mathbf{r})\frac{\partial T(\mathbf{r})}{\partial n} \quad (2)$$

where  $H$ ,  $T_s$ , and  $T_e$  denote, respectively, the heat transfer coefficient, the surface temperature of the tissue, and the temperature of the air. The finite-difference expressions for (1) and (2) are given in [4], [6]. Note that this paper does not treat the temperature increase due to the altered heat transfer mechanism due to the presence of handset terminal. Detailed discussion on this subject can be found in [25].

## III. NUMERICAL RESULTS

### A. Basic Theory for Temperature Increase

The temperature increase in the human model due to EM waves becomes maximum at the thermally steady state. For this reason, the temperature increase at the thermally steady state is considered in this paper. The bioheat equation and its boundary condition are reduced to the following equations at the thermally steady state:

$$\{\nabla \cdot (K(\mathbf{r})\nabla) - B(\mathbf{r})\}\delta T(\mathbf{r},t) = -\rho(\mathbf{r})\text{SAR}(\mathbf{r}) \quad (3)$$

$$\left(H + K(\mathbf{r})\frac{\partial}{\partial n}\right)\delta T(\mathbf{r},t) = 0 \quad (4)$$

where  $\delta T(\mathbf{r})$  is the temperature increase of tissue. Eq. (3) is a linear differential equation subject to boundary conditions. Namely, the temperature increase is linear in terms of SAR.

<sup>1</sup>www.fcc.gov/fcc-bin/dielec.sh

TABLE I  
THERMAL CONSTANT AND MASS DENSITY OF HUMAN TISSUES.

	$K$ W/m $\cdot$ °C	$C_p$ J/kg $\cdot$ °C	$\rho$ kg/m $^3$	$B$ W/°C $\cdot$ m $^3$	$A$ W/m $^3$
skin	0.42	3600	1125	9100	1620
muscle	0.50	3800	1047	2700	480
fat	0.25	3000	916	1700	300
bone	0.37	3100	1990	3400	610
cartilage	0.47	3600	1097	9000	1600
bone marrow	0.22	3000	1040	32000	5700
gray matter	0.57	3800	1038	40000	7100
white matter	0.50	3500	1038	40000	7100
cerebellum	0.57	3800	1038	40000	7100
CSF	0.62	4000	1007	0	0
humor	0.58	4000	1009	0	0
cornea	0.58	3800	1076	0	0
lens	0.40	3600	1053	0	0
sclera	0.58	3800	1026	0	0
heart	0.54	3900	1030	54000	9600
liver	0.51	3700	1030	68000	12000
lung	0.14	3800	260	9500	1700
kidneys	0.54	4000	1050	270000	48000
intestine(small)	0.57	4000	1043	71000	13000
intestine(large)	0.56	3900	1043	53000	9500
gall bladder	0.47	3900	1030	9000	1600
spleen	0.54	3900	1054	82000	15000
stomach	0.53	4000	1050	29000	5200
pancreas	0.54	4000	1045	41000	7300
blood	0.56	3900	1058	0	0
blood vessel	0.56	3900	1040	9100	1620
body fluid	0.56	3900	1010	0	0
glands	0.53	3500	1050	360000	64000
ligaments	0.50	3600	1220	9000	1600
membrane	0.50	3600	1040	9000	1600
2/3muscle	0.39	3160	1000	-	408

It should be noted that  $Q$  and  $C$  do not affect the temperature increase at the thermally steady state. Let us consider this problem on the basis of a Green's function. The Green's function satisfies the following equations:

$$L(\mathbf{r})G(\mathbf{r}; \mathbf{r}_i) = -\delta(\mathbf{r} - \mathbf{r}_i) \quad (5)$$

$$L(\mathbf{r}) = \nabla \cdot (K(\mathbf{r})\nabla) - B(\mathbf{r}) \quad (6)$$

where  $G(B(\mathbf{r}; \mathbf{r}_i), K(\mathbf{r}; \mathbf{r}_i), H)$  is a Green's function associated with the differential operator  $L$ . The Green's function is dependent on the blood flow and heat conductivity, together with the heat transfer coefficient corresponding to air temperature (See Eq. (2)).

The temperature increase at a particular position is given in the discretized form as:

$$\delta T(\mathbf{r}) = \sum_i \rho(\mathbf{r}_i) S A R(\mathbf{r}_i) G(B(\mathbf{r}; \mathbf{r}_i), K(\mathbf{r}; \mathbf{r}_i), H). \quad (7)$$

Note that the equation in [16] is reduced to this equation at the thermally-steady state. For investigating steady-state temperature increase, it would be essential to investigate the Green's function itself for understanding the length that heat can diffuse. Then, a one-dimensional infinite homogeneous model is considered. Additionally, a semi-infinite model is considered to evaluate the effect of boundary between air and tissue. Note that discussion using a different approach can be found in [26]. Then, point heat potential (50 W/m $^2$ ) is given at the origin ( $x=0$ ) in Fig. 3. Figures 3 (a) and (b) show the

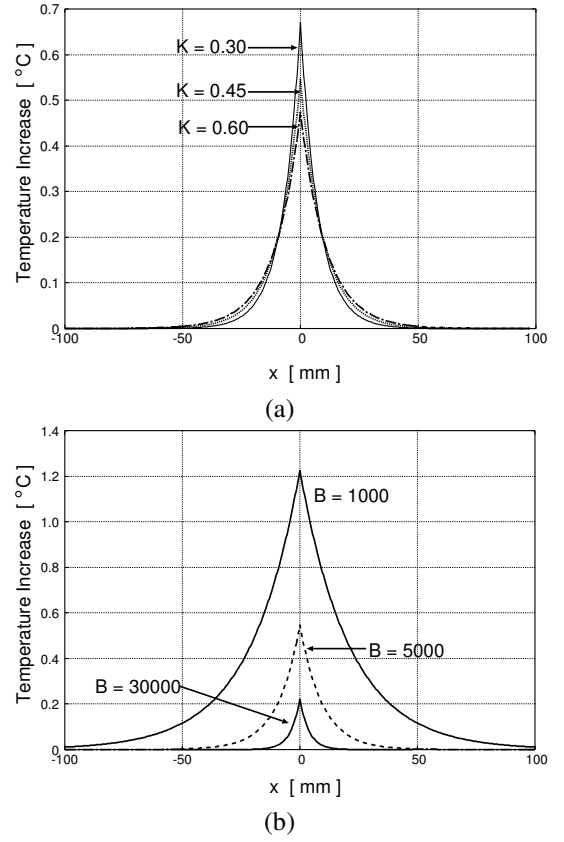


Fig. 3. Temperature increase distribution in the 1-D slab for (a) different heat conductivity (with  $B = 5000$  W/m $^3$ ·°C), (b) different term associated with blood flow (with  $K = 0.45$  W/m·°C).

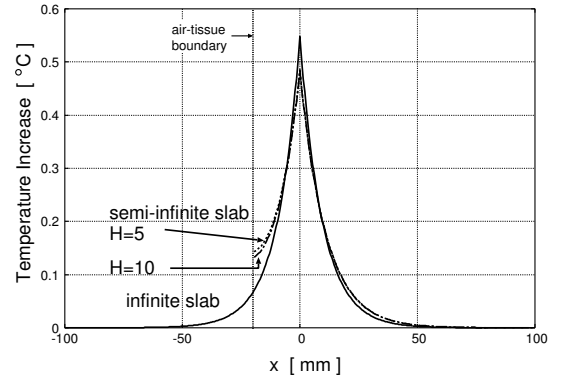


Fig. 4. Temperature increase distribution in the semi-infinite 1-D slab with  $B = 5000$  W/m $^3$ ·°C and  $K = 0.45$  W/m·°C.

temperature increase distribution in the slab for (a) different heat conductivities (with  $B = 5000$  W/m $^3$ ·°C) and (b) different terms associated with blood flow (with  $K = 0.45$  W/m·°C). Note that heat conductivities of tissues are in the range from 0.3 (~ fat) to 0.6 W/m·°C (~ humor). The terms of blood flow for human tissues are in the range from 1000 (~ fat) to 30000 W/m $^3$ ·°C (~ brain). Comparing Figs. 3(a) and (b), the effect of blood flow of tissue on the temperature increase distribution is much larger than that of heat conductivity. In addition, the distance that the heat can diffuse is also larger for smaller term associated with blood flow rate. Figure 4 illustrates the

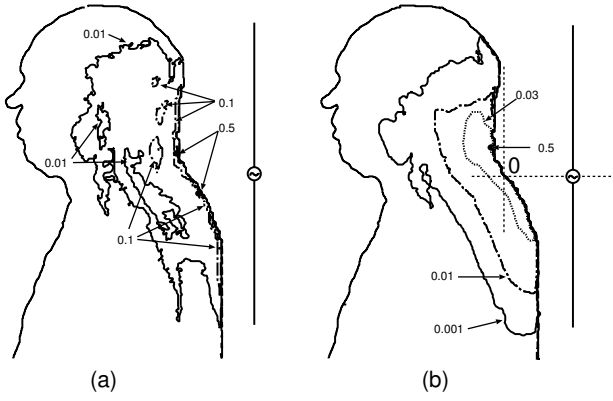


Fig. 5. SAR (a) and temperature increase (b) distributions on midsagittal vertical cross section. The antenna feeding position is 54 mm behind the neck.

TABLE II

PEAK 10-G SAR [W/kg] AND MAXIMUM TEMPERATURE INCREASE [°C] DUE TO THE DIPOLE ANTENNA BEHIND THE NECK:  $d =$  (a) 54 mm, (b) 84 mm, AND (c) 114 mm.

		peak SAR	max. $\Delta T$
(a)		0.45	0.11
	position	(3, -24, -57)	(3, -21, -54)
(b)		0.23	0.059
	position	(12, -24, -45)	(12, -24, -42)
(c)		0.12	0.030
	position	(15, -24, -45)	(15, -24, -42)

temperature increase distribution for a semi-infinite slab. The heat transfer coefficient is set to  $10.5 \text{ W/m}^2 \cdot ^\circ\text{C}$  [27].

The air-tissue boundary exists at  $x = 20 \text{ mm}$ . From this figure, the effect of heat transfer coefficient on the temperature increase is comparable to that due to heat conductivity of tissue. Namely, the effect of blood flow on the temperature increase is essential to determine the temperature increase [28], [29]. Then, Eq. (7) is approximately simplified to the following equation:

$$\delta T(\mathbf{r}) \simeq \sum_i \rho(\mathbf{r}_i) \text{SAR}(\mathbf{r}_i) G(B(\mathbf{r} - \mathbf{r}_i)). \quad (8)$$

### B. SAR and Temperature Increase Due to Antenna in Proximity to Human Body

Figure 5 illustrates the SAR and temperature increase distributions at the antenna-body distance of 54 mm. The antenna is located behind the neck. Comparing these distributions, the temperature-rise distribution is largely affected by the SAR distribution. Then, the former is not linearly proportional to the latter. In particular, the temperature rise distribution is much smoother than the SAR distribution. This is because of heat diffusion, which is governed by the bioheat equation. These results are consistent with the results in previous articles [4], [5], [6], [7], [9], which investigate the temperature increase in the head due to a handset antenna.

Table II lists the peak spatial-average SAR and maximum temperature increase at  $d = 54, 84, 114 \text{ mm}$ . Note that 54 mm corresponds to a minimum distance, which does not make the antenna touched to the human body for the case where the antenna is placed behind the neck. The position of peak SAR is

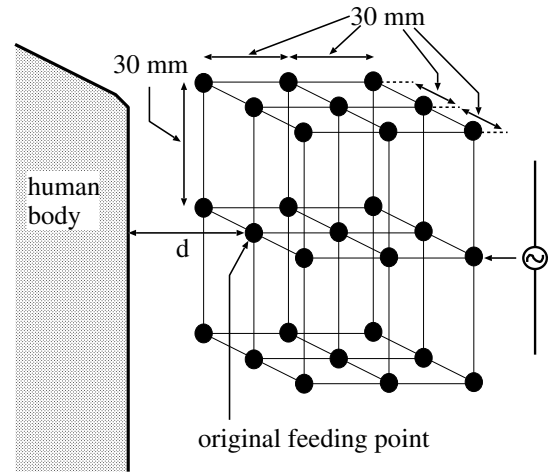


Fig. 6. Positions of antenna feeding point relative to human body.

defined as that of the center voxel in the volume for averaging SAR. Note that the position has the unit of mm, and the origin is defined in Fig. 2 (b). For calculating peak SAR, the scheme specified by the IEEE standard [24] is used. Namely, the shape of averaging volume is a cube. The averaging mass is 10 g. The positions of peak SAR and maximum temperature increase are in excellent agreement. This is also true for the cases where the antenna is located behind the back and waist, although not shown here for avoiding repetition. For handset antennas placed in close proximity of the head, the positions of peak SAR and maximum temperature increase were not always coincident [10]. Such phenomena are not observed for the cases considered in this paper. This is attributed to relatively simple shape of the trunk, unlike the shape of the pinna where handset antennas are used.

The correlation between peak spatial-average SAR and maximum temperature increase is discussed for the dipole antenna at 400 MHz. For this purpose, the total of 27 feeding positions is considered for each body part, as shown in Fig. 6. For each feeding positions, peak SAR versus maximum temperature increase are plotted in Fig. 7. As is evident from this figure, strong correlation between peak SAR and maximum temperature increase is observed for each antenna position. The coefficients of determination, which characterize the magnitude of the correlation, are 0.960, 0.988, 0.988 for the neck, waist, and back, respectively. Namely, the less the observed values depart from the fitted line, the closer to unity the coefficient is. It is noteworthy that the slopes for the neck and back are in good agreement, while that of the back is somewhat smaller than that of the other cases.

In order to discuss quantitatively, Table III lists the slope of the regression line for all cases considered in this paper. The coefficients of determination are not listed, since they are close to unity for all cases. From this table, the slope of the regression line is only marginally affected by different frequencies and antennas ( $< 10\%$ ). When the antennas are located behind the neck, the slopes are almost identical except for the monopole antenna at 900 MHz. We attribute a main reason for this difference to tissues where maximum

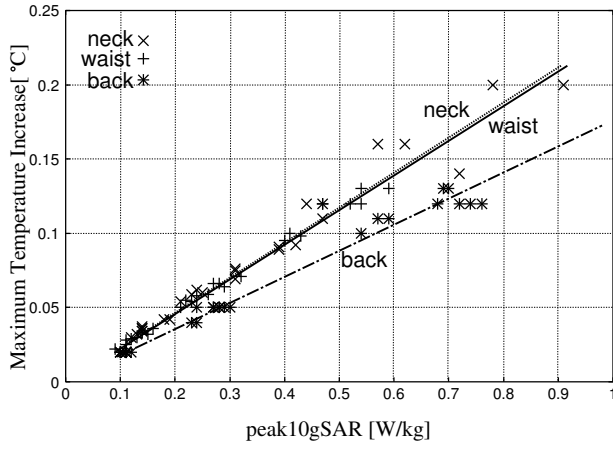


Fig. 7. Peak spatial-average SAR and maximum temperature increase for different antenna positions at 400 MHz.

TABLE III

SLOPES OF REGRESSION LINE FOR (A) DIPOLE AND (B) MONOPOLE ANTENNAS AT 400 AND 900 MHz, AND (C) HELICAL ANTENNA AT 150 AND 400 MHz.

(a)		
frequency	400MHz	900MHz
neck	0.239	0.254
waist	0.235	0.218
back	0.177	0.184

(b)		
frequency	400MHz	900MHz
neck	0.257	0.189
waist	0.233	0.221
back	0.194	0.190

(c)		
frequency	150MHz	400MHz
neck	0.242	0.230
waist	0.215	0.220
back	0.181	0.175

temperature increases appear. Specifically, this is caused by the difference in the blood flow of tissues (see Eq. (8)). For the monopole antenna at 900 MHz, the maximum temperature increase appears in the skin ( $B = 9100 \text{ W/m}^3 \cdot ^\circ\text{C}$ ), while in the muscle ( $B = 2700 \text{ W/m}^3 \cdot ^\circ\text{C}$ ) or fat ( $B = 1700 \text{ W/m}^3 \cdot ^\circ\text{C}$ ) for the other cases. This would occur because peak SAR appears around the neck for the monopole antenna at 900 MHz due to the existence of metallic box. Note that the slope of the regression line for this case agrees well for the cases when the antenna is attached to the back.

In order to further investigate the difference in the slope of the regression line which is caused by antenna positions, the effect of blood flow on the correlation is discussed. Note that our attention is concentrated on the effect of blood flow. This is because the correlation is little affected by the heat conductivity, specific heat as discussed in Sec. 3.1. Additionally, we have presented that the effect of relative permittivity and conductivity of tissues is also marginal [29]; at most a few percent due to a variation by 50 % for each parameter. The realistic human body model is *homogenized*

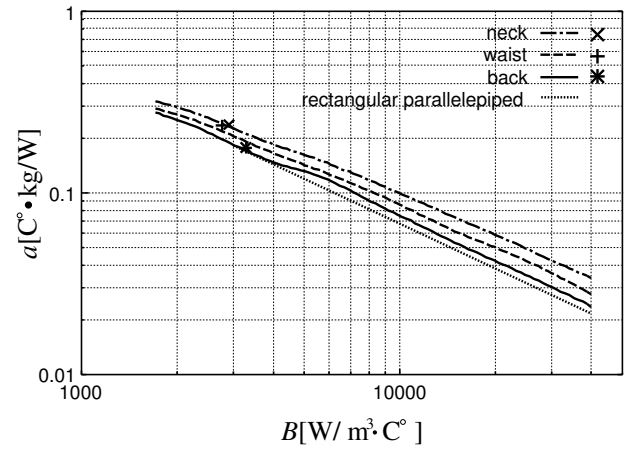


Fig. 8. Influence of blood flow of tissue on the slope of the regression line for different body parts. The frequency is 400 MHz. The points correspond the results using the inhomogeneous model.

as a 2/3 muscle. Only blood flow of the tissue is considered as a variable. Figure 8 shows the dependency of the slope correlating the maximum temperature increase and peak SAR on the local blood flow. The dipole antenna at 400 MHz is used. For comparison, the results using the inhomogeneous model are also plotted. Note that we define the blood flow for the inhomogeneous model as the value averaged over the volume for calculating peak spatial-average SAR. The model of rectangular parallelepiped is also used to discuss the effect of model shape. The dimensions of this rectangular parallelepiped are 513 mm ( $x$ )  $\times$  333 mm ( $y$ )  $\times$  633 mm ( $z$ ). From this figure, the slopes are almost coincident for the three antenna positions. The difference in the slope caused by the antenna position is up to 30%. One of the main reasons for this difference is attributed to the body shape around the source. The shape around the back is almost flat and resembles the rectangular parallelepiped. Another point to be stressed is that the results for the inhomogeneous model, which are represented as points, are reasonably on the curves. From this coincidence, the slopes are found to be largely affected by blood flow around the position where peak SAR appears.

Figure 9 illustrates the effect of different antennas and frequencies on the slope of the regression line for different antenna positions. In Fig. 9(a), three curves except for that of the monopole antenna at 900 MHz are in good agreement. The reason for this agreement is the difference in positions where peak SAR and maximum temperature increase appear. From Figs. 9 (b) and (c), the effect of different antennas and frequencies is marginal, since all curves considered are well coincident with one another in each figure. These results emphasize that blood flow around the position where peak SAR appears is one of the most dominant factors to determine the slopes correlating peak SARs and maximum temperature increases. Namely, Figure 9 suggests that our interpretation can be extended to different blood flow. Based on these figures, we can roughly estimate the maximum temperature increase using peak spatial-average SAR and average blood flow. For accurate estimation of a maximum temperature increase, temperature calculation using an inhomogeneous model

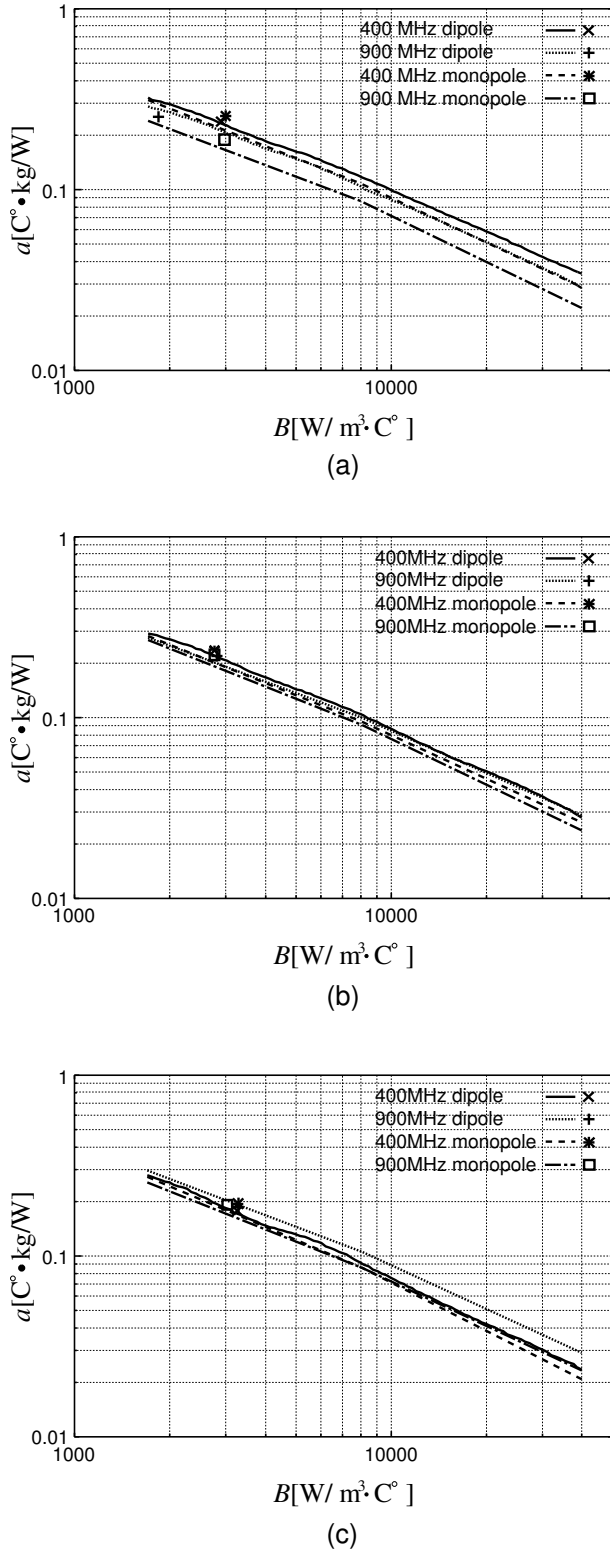


Fig. 9. Influence of blood flow of tissue on the slope of the regression line for different antennas and frequencies.

is required.

Let us discuss a possible temperature increase at peak 10-g SAR of 10 W/kg, which is the limit in the safety guidelines. From Fig. 8, the slope of the regression line is  $0.3 \text{ }^{\circ}\text{C} \cdot \text{kg/W}$  for blood flow of  $1500 \text{ W/m}^3 \cdot ^{\circ}\text{C}$ . This is the smallest value of the term associated with blood flow except for fat. Then, possible temperature increase is around  $3 \text{ }^{\circ}\text{C}$ . The temperature at the human trunk is  $34 \text{ }^{\circ}\text{C}$  at ambient temperature of  $25 \text{ }^{\circ}\text{C}$  [30]. Thus, possible maximum temperature is lower than  $37 \text{ }^{\circ}\text{C}$  at the surface. This temperature might increase the blood flow in the skin, but marginal [32]. Also note that  $39 \text{ }^{\circ}\text{C}$  is a threshold temperature to activate the thermoregulatory mechanism of the inner tissue [31]. Maximum temperature increase appears around 1 cm inside from the skin. At this depth, the temperature is  $36 \text{ }^{\circ}\text{C}$  or so. Then, at the SAR limit for occupational environment, thermoregulatory mechanism might be activated, but not so significant as is the case of the skin.

#### IV. SUMMARY

This paper investigated the SAR and temperature increase for the trunk-mounted antenna at 400 MHz and 900 MHz bands. For the basic case, one-dimensional model has been considered for investigating the effect of variation of thermal constants on the temperature increase. In order to generalize this problem, a Green's function is used. This investigation has suggested that one of the most dominant factors which affect the correlation between peak SARs and maximum temperature increases is blood flow. For the 3-D realistic human model developed by the Brooks AFB, strong correlation was observed between peak SAR and maximum temperature increase in the body, as is the case with EM wave exposures from handset antennas. The variation of slope of regression line caused by the model shape was 20-30%. The effect of different antennas and frequencies on this correlation was smaller than that by the model shape (less than 10%). Furthermore, it was confirmed that the decisive factor which determines the temperature increase is blood flow around the position where peak SAR appears. Based on the relation between the slope of regression line and the blood flow, we can roughly estimate the maximum temperature increase using peak spatial-average SAR. For more proper estimation of maximum temperature increase, temperature calculation using a inhomogeneous model would be essential.

Future works are required for other human body models, such as child and female in order to validate the results in this paper.

#### REFERENCES

- [1] International Commission on Non-Ionizing Radiation Protection (IC-NIRP), "Guidelines for limiting exposure to time-varying electric, magnetic and electromagnetic fields (up to 300 GHz)," *Health Phys.*, vol.74, pp.494-522, 1998.
- [2] J. D. Hardy, "The nature of pain," *J. Chronic. Dis.*, vol.4, no.22, 1956.
- [3] E. R. Adair, B. W. Adams, and G. M. Akel, "Minimal changes in hypothalamic temperature accompany microwave-induced alteration of thermoregulatory behavior," *Bioelectromagnetics*, vol.5, pp.13-30, 1984.
- [4] J. Wang and O. Fujiwara, "FDTD computation of temperature rise in the human head for portable telephones," *IEEE Trans. Microwave Theory & Tech.*, vol.47, pp.1528-1534, 1999.



- [5] G. M. J. Van Leeuwen, J. J. W. Lagendijk, B. J. A. M. Van Leersum, A. P. M. Zwamborn, S. N. Hornsleth, and A. N. T. Kotte, "Calculation of change in brain temperatures due to exposure to a mobile phone," *Phys. Med. Biol.*, vol. 44, pp.2367-2379, 1999.
- [6] P. Bernardi, M. Cavagnaro, S. Pisa, and E. Piuze, "Specific absorption rate and temperature increases in the head of a cellular-phone user," *IEEE Trans. Microwave Theory & Tech.*, vol.48, pp.1118-1126, 2000.
- [7] P. Wainwright, "Thermal effects of radiation from cellular telephones," *Phys. Med. Biol.*, vol.45, pp.2363-2372, 2000.
- [8] P. Gandhi, Q.-X. Li, and G. Kang, "Temperature rise for the human head for cellular telephones and for peak SARs prescribed in safety guidelines," *IEEE Trans. Microwave Theory & Tech.*, vol.49, no.9, pp.1607-1613, Sep. 2001.
- [9] A. Hirata, M. Morita, and T. Shiozawa, "Temperature increase in the human head due to a dipole antenna at microwave frequencies," *IEEE Trans. Electromagnet.Compat.*, vol.45, no.1, pp.109-116, Feb. 2003.
- [10] A. Hirata and T. Shiozawa, "Correlation of maximum temperature increase and peak SAR in the human head due to handset antennas," *IEEE Trans. Microwave Theory & Tech.*, vol.51, no.7, pp.1834-1841 July 2003.
- [11] S. S. Stuchly, A. Kraszewski, M. A. Stuchly, G. Hartsgrrove, and D. Adamski, "Energy deposition in a model of man in the near field," *Bioelectromagnetics*, vol.6 pp.115-129, 1985.
- [12] I. Chatterjee, Y.-G. Gu, and O. P. Gandhi, "Quantification of Electromagnetic absorption in humans from body-mounted communication transceivers," *IEEE Trans. Vehicular Tech.*, vol.34, no.2, pp.55-62, May 1985.
- [13] H.-R. Chuang and W.-T. Chen, "Computer simulation of the human-body effects on a circular-loop-wire antenna for radio-pager communications at 152, 280, and 400 MHz," *IEEE Trans. Vehich. Tech.*, vol.46, no.3, pp.544-559, 1997.
- [14] W. Chamma, S. Kashyap, and A. Louie, "EM fields in a human body due to a manpack transceiver for different soil conditions," *Proc. IEEE Electromagnetc. Compat.*, pp.1066-1071,2001.
- [15] J. V. Beck, K. D. Cole, A. Haji-Sheikh, and B. Litkouh, Heat conduction using Green Functions, Hemisphere (Washington DC), 1992.
- [16] Z.-S. Deng and J. Liu, "Analytical study on bioheat transfer problems with spatial or transient heating on skin surface or inside biological bodies," *Trans. ASME J. Biomecha. Eng.*, vol.124, pp.638-649, 2002.
- [17] [ftp://starview.brooks.af.mil/EMF/dosimetry\\_models](ftp://starview.brooks.af.mil/EMF/dosimetry_models)
- [18] A. Taflov and S. Hagness, *Computational Electrodynamics: The Finite-Difference Time-Domain Method: 2nd Ed.*, Norwood, MA: Artech House, 1998.
- [19] C. Gabriel, "Compilation of the dielectric properties of body tissues at RF and microwave frequencies," *Final Technical Report Occupational and Environmental Health Directorate AL/OE-TR-1996-0037* (Brooks Air Force Base, TX: RFR Division).
- [20] S. Watanabe and M. Taki, "An improved FDTD model for the feeding gap of a thin-wire antenna," *IEEE Microwave and Guided Wave Letts.*, vol.8, no.4, pp.152-154, Apr. 1998.
- [21] G. Lazzi and O. P. Gandhi, "On modeling and personal dosimetry of cellular telephone helical antennas with the FDTD code," *IEEE Trans. Antennas & Propagat.*, vol.46, no.4, pp.525-529, Apr. 1999.
- [22] H. H. Pennes, "Analysis of tissue and arterial blood temperature in resting forearm," *J. Appl. Physiol.* Vol.1, pp.93-122, 1948.
- [23] J. A. J. Stolwijk and J. D. Hardy, "Temperature regulation in man - A theoretical study," *Pflugers Arch.*, vol.291, pp.129-162, 1966.
- [24] IEEE C95.3-2002 Standard, Annex E, 2002.
- [25] A. Ibrahim, C. Dale, W. Tabbara, and J. Wiart, "Analysis of the temperature increase linked to the power induced by RF source," *Progress in Electromagnetic Res.*, vol.52, pp.23-46, 2005.
- [26] K. R. Foster, H. N. Kritikos, and H. P. Schwan, "Effect of surface cooling and blood flow on the microwave heating of tissue," *IEEE Trans. Biomed. Eng.*, vol.23, no.3, pp.313-316, 1978.
- [27] H. N. Kritikos, K. R. Foster, and H. P. Schwan, "Temperature profiles in spheres due to electromagnetic heating," *J. Microwave Power*, vol.16, nos.3/4, pp.327-344, 1981.
- [28] K. Iino, O. Fujiwara, K. Katoh, and T. Azakami, "Numerical calculation of temperature rise inside human head irradiated by RF electromagnetic fields under ANSI safety guide," *IEICE Trans.* vol.J72-B-II, no.2, pp.81-83, 1998 (in Japanese).
- [29] M. Fujimoto, A. Hirata, J. Wang, O. Fujiwara, and T. Shiozawa, "Comparison of maximum temperature increase in the head models of children and adult due to dipole antenna," *IEEE Topical Conf. Wireless Commun. Tech.*, 14-2, Oct. 2003 (Hawaii, USA).
- [30] W. F. Ganong, Review of Medical Physiology: 21th Ed., Large Medical Books/McGraw Hill:NY, 2003.
- [31] M. Hoque and O. P. Gandhi, "Temperature distributions in the human leg for VLF-VHF exposures at the ANSI recommended safety levels," *IEEE Trans. Biomed. Eng.*, vol.35, no.6, pp.442-449, 1988.
- [32] D. H. K. Lee, Ed., Handbook of Physiology-Reaction to Environmental Agents, Ame. Physiol. Soc., Bethesda: MD, 1977.



**Akimasa Hirata** was born in Okayama, Japan, on November 27, 1973. He received the B.E., M.E., Ph.D degrees in communication engineering from Osaka University, Suita, Osaka, Japan, in 1996, 1998, and 2000, respectively. He was a research fellow of the Japan Society for the Promotion of Science for the 1999-2001 period and also a visiting research scientist in the University of Victoria, Canada from May to October in 2000. In 2001, he joined the Department of Communications Engineering, Osaka University as an Assistant Professor. In 2005,

he joined the Department of Computer Science and Engineering, Nagoya Institute of Technology as an Associate Professor. His research interests are in electron beam devices for high-power millimeter or submillimeter generation, bioelectromagnetics, waveguide analysis, and computational techniques in electromagnetics.

Dr. Hirata won several awards, including the young scientist award (URSI Commission B in 2001), the young scientist award (the Ericsson in 2001), the young engineer award, and Telecom System Technology Award (Telecommunications Advancement Foundation in 2004).



**Osamu Fujiwara** received the B.E. degree in electronic engineering from the Nagoya Institute of Technology, Nagoya, Japan, in 1971, and the M.E. and the D.E. degrees in electrical engineering from Nagoya University, Nagoya, Japan, in 1973 and in 1980, respectively.

From 1973 to 1976, he was with the Central Research Laboratory, Hitachi Ltd., Kokubunji, Japan, where he was engaged in research and development of system packaging designs for computers. From 1980 to 1984, he was with the Department of Electrical Engineering, Nagoya Institute of Technology, where he is currently a Professor. His research interests include measurement and control of electromagnetic interference due to discharge, bioelectromagnetics, and other related areas of electromagnetic compatibility.



**Toshiyuki Shiozawa** was born in Tokyo, Japan, on January 16, 1941. He received the B. E., M. E. and Ph. D. degrees in communication engineering from Osaka University, Suita, Osaka, Japan in 1964, 1966 and 1969, respectively. In 1969 he joined the Department of Communication Engineering, Osaka University, where he is now a Professor.

He has been engaged in the research of relativistic electromagnetic theory for engineering-oriented applications, and theoretical study of free-electron lasers. His current research interests include nonlinear electromagnetics and bioelectromagnetics. He served also as an Associate Editor of the IEICE Transactions on Electronics from 1995 to 1999. He was the Chairman of the Technical Committee on Electromagnetic Theory in IEE Japan from 1999 to 2002. In 2000, he organized the Japan-China Joint Meeting on Optical Fiber Science and Electromagnetic Theory. He is a co-author of the books *Topics in Advanced Electromagnetic Theory* (Tokyo, Japan: Corona, 1988) and *Exercise in Electromagnetic Theory* (Tokyo, Japan: Corona, 1998). In 2001, he was elected to the grade of IEEE Fellow for contributions to engineering-oriented relativistic electromagnetic theory and theoretical study of free-electron lasers.